

Fragmentation Functions for $\Xi^-/\bar{\Xi}^+$ Using Neural Networks

Maryam Soleymaninia^{1,*}, Hadi Hashamipour^{1,†}, Hamzeh Khanpour^{2,3,4,1,‡} and Hubert Spiesberger^{5,§}

¹*School of Particles and Accelerators, Institute for Research in Fundamental Sciences (IPM), P.O.Box 19395-5531, Tehran, Iran*

²*Dipartimento Politecnico di Ingegneria ed Architettura, University of Udine, Via della Scienze 206, 33100 Udine, Italy*

³*International Centre for Theoretical Physics (ICTP), Strada Costiera 11, 34151 Trieste, Italy*

⁴*Department of Physics, University of Science and Technology of Mazandaran, P.O.Box 48518-78195, Behshahr, Iran*

⁵*PRISMA⁺ Cluster of Excellence, Institut für Physik, Johannes-Gutenberg-Universität, Staudinger Weg 7, D-55099 Mainz, Germany*

(Dated: November 1, 2022)

We present a determination of fragmentation functions (FFs) for the octet baryon $\Xi^-/\bar{\Xi}^+$ from data for single inclusive electron-positron annihilation. Our parametrization in this QCD analysis is provided in terms of a Neural Network (NN). We determine fragmentation functions for $\Xi^-/\bar{\Xi}^+$ at next-to-leading order and for the first time at next-to-next-to-leading order in perturbative QCD. We discuss the improvement of higher-order QCD corrections, the quality of fit, and the comparison of our theoretical results with the fitted datasets. As an application of our new set of fragmentation functions, named **SHKS22**, we present predictions for $\Xi^-/\bar{\Xi}^+$ baryon production in proton-proton collisions at the LHC experiments.

CONTENTS

I	Introduction	1
II	QCD Framework	2
III	Methodology and Input Parameterization	3
IV	Monte Carlo Procedure and Determination of the Optimal Fit	4
V	Experimental Data	5
VI	FF Sets and Fit Quality	5
VII	$\Xi^-/\bar{\Xi}^+$ Production at Hadron Colliders	8
VIII	Summary and Conclusions	10
	Acknowledgments	12
	References	13

I. INTRODUCTION

Fragmentation Functions (FFs) are necessary to describe the hadronization process in which partons turn into hadrons in the final state. They are needed to describe hadron production in semi-inclusive processes in electron-positron annihilation (SIA), and, together

with parton distribution functions (PDFs) in lepton nucleon scattering and (anti)proton-proton collisions. Parametrizations of FFs for light hadrons, as well as for mesons with charm and bottom quarks, are available since long and the corresponding phenomenology is well established. New improved data are routinely used to improve the existing FF parametrizations, see for example [1, 2] and references therein. In recent years, progress has been made also for more specific applications, as for example the determination of transverse momentum dependent FFs [3, 4], FFs for heavier hadrons, like Λ_c^\pm baryons [5] and medium modified FFs [6]. With more precise data it seems also possible to aim at a combined determination of PDFs and FFs [7] and future experiments, for example at the EIC [8], will eventually improve our understanding of FFs.

In this work we are interested in a determination of FFs for the production of Ξ^- and its anti-particle, i.e. the double-strangeness carrying octet baryon. On the experimental side, most important information about Ξ^- production is coming from SIA measurements in e^+e^- annihilation on the Z -boson resonance at the LEP experiments ALPEH [9], DELPHI [10] and OPAL [11]. Earlier data are also available from MARKII [12] and TASSO [13, 14] at somewhat smaller center-of-mass energies. In recent years, also data for Ξ^- -production in pp and $\bar{p}p$ collisions have been published, covering center-of-mass energies from $\sqrt{s} = 17.3$ GeV at NA61/SHINE [15], $\sqrt{s} = 200$ GeV at STAR [16, 17], 1.96 TeV at CDF [18], and up to 7 and 13 TeV at CMS [19, 20] and ALICE [21–23]. The relevant energy scale in these collider experiments is the transverse momentum of the produced hadron which is, however, rather low and does not reach values above 10 GeV.

On the theoretical side, the only available analysis of the FF of the Ξ^- was made in a statistical approach and used data from e^+e^- annihilation [24]. This motivates us

* Maryam_Soleymaninia@ipm.ir

† H_Hashamipour@ipm.ir

‡ Hamzeh.Khanpour@cern.ch

§ spiesber@uni-mainz.de

to perform a new determination of the Ξ^- FF using the by now well established technique of neural networks.

The main motivation of our present study is to determine a new set of $\Xi^-/\bar{\Xi}^+$ FFs. The universality property of FFs allows us to perform a QCD analysis using all available measurements to determine the FFs for a specific hadron. The FFs extracted in this way can be used to obtain theoretical predictions for other processes, like hadron production in pp collisions. In this paper we present a determination of the FFs of $\Xi^-/\bar{\Xi}^+$ baryon in which single inclusive electron-positron annihilation (SIA) data are analyzed at next-to-leading order (NLO) and next-to-next-to-leading order (NNLO) accuracy in perturbative QCD.

We hope that our determination of $\Xi^-/\bar{\Xi}^+$ FFs will provide the necessary ingredient needed to obtain predictions for future measurements in a well-defined reference framework based on independent parton-to-hadron fragmentation in perturbative QCD. Such a reference will be needed to test theoretical ideas about mechanisms for hadron production. With future precise data, a comparison with predictions from perturbative QCD is expected to reveal non-perturbative mechanisms and possible collective phenomena in a high-temperature quark-gluon plasma (QGP). For instance, one of the signatures for creating a QGP is production of strange hadrons in heavy-ion collisions [25, 26]. In particular hadrons with low transverse momentum are expected to reflect the properties of the bulk system such as collective expansion, the hadro-chemical composition, and the temperature at freeze-out. Measurements of identified hadrons at low transverse momentum used to extract these properties [27, 28] will also profit from theory predictions for higher transverse momenta obtained in a reference framework.

We use the recent publicly available **MontBlanc** package [29] in our analysis. This package is based on neural networks which are believed to provide a parametrization with minimal bias. This allows us to control the precision of the $\Xi^-/\bar{\Xi}^+$ FFs, based on an efficient minimization algorithm. The numerical calculations of the hadron production cross-section in e^+e^- annihilation and the scale evolution of the FFs is also performed in this framework. The fitting methodology in the framework of this package has been developed by the NNPDF Collaboration [1, 30, 31].

We will discuss in detail the novel aspects of the methodology used in SHKS22 analysis, the fit quality, the perturbative convergence upon inclusion of higher-order QCD correction, and the stability upon variations of the kinematic cuts applied to the SIA dataset. We will also show that the inclusion of higher-order QCD corrections in our analysis improves the description of the analyzed SIA data.

The structure of the paper is as follows: In Sec. II we review the theoretical formalism for inclusive hadron production in electron-positron annihilation. In Sec. III our methodology based on a neural network (NN) framework

is presented. We illustrate the Monte Carlo methodology adopted in our analysis to calculate the uncertainties of FFs and the optimal fit in Sec. IV. In Section V we describe our selection of SIA experimental data included in this study. Details of our new SHKS22 FFs are presented in Sec. VI. We also discuss in this section the impact of higher-order perturbative QCD (pQCD) corrections and compare numerical results for the differential cross sections with the analyzed experimental datasets. In Sec. VII, we present and discuss some predictions for possible future measurements at hadron colliders. Finally, we summarize our conclusions in Sec. VIII.

II. QCD FRAMEWORK

For single inclusive hadron production in electron-positron annihilation, the differential cross-section is given by the formula

$$\frac{d\sigma^h}{dz}(z, Q^2) = \frac{4\pi\alpha^2(Q)}{Q^2} F^h(z, Q^2), \quad (1)$$

where F^h is the fragmentation structure function, and α is the QED running coupling¹. We follow the standard collinear factorization framework [33] where the QCD cross-sections can be factorized into perturbatively calculable partonic hard cross sections and non-perturbative distribution functions. Thus the structure function is given as a convolution of FFs and hard-scattering coefficient functions:

$$F^h(z, Q^2) = \frac{1}{n_f} \sum_q^{n_f} \hat{e}_q^2(Q) \times \left[D_S^h(z, Q^2) \otimes C_{2,q}^S(z, \alpha_s(Q)) + D_g^h(z, Q^2) \otimes C_{2,g}^S(z, \alpha_s(Q)) + D_{NS}^h(z, Q^2) \otimes C_{2,q}^{NS}(z, \alpha_s(Q)) \right], \quad (2)$$

where $\hat{e}_q(Q)$ are scale-dependent quark electroweak charge factors. Their definition can be found in Ref. [34]. In Eq. (2), the function $D_g^h(z, Q^2)$ represents the gluon FF, and $D_S^h(z, Q^2)$ and $D_{NS}^h(z, Q^2)$ are the singlet and non-singlet combinations of FFs which can be written as

$$D_S^h(z, Q^2) = \sum_q^{n_f} D_{q^+}^h(z, Q^2), \quad (3)$$

$$D_{NS}^h(z, Q^2) = \sum_q^{n_f} \frac{\hat{e}_q^2}{\langle \hat{e}^2 \rangle} \left[D_{q^+}^h(z, Q^2) - D_S^h(z, Q^2) \right], \quad (4)$$

¹ We follow the convention of Ref. [32] where the combination of the transverse and longitudinal fragmentation structure functions $F^h = F_T^h + F_L^h$ is used. This is the combination which can be determined after integrating over the hadron's emission angle with respect to the beam direction. Sometimes F^h is also denoted F_2^h in the literature, see e.g. Ref. [31].

with $D_{q^+}^h = D_q^h + D_{\bar{q}}^h$. The coefficient functions $C_{q,g}^{S,NS}(z, \alpha_s(Q))$ for the singlet and non-singlet combinations have been computed up to $\mathcal{O}(\alpha_s^2)$ [35, 36]. The average of the effective quark electroweak charges over the number of active flavors reads

$$\langle \hat{e}^2 \rangle = \frac{1}{n_f} \sum_q^{n_f} \hat{e}_q^2(Q). \quad (5)$$

The evolution of FFs with the energy scale Q is performed by the standard DGLAP evolution equation [37–39]. The evolution of the singlet combination of FFs mixes with the gluon FF and is given by

$$\begin{aligned} \frac{\partial}{\partial \ln Q^2} \begin{pmatrix} D_S^h \\ D_g^h \end{pmatrix} (z, Q^2) &= \begin{pmatrix} P^{qq} & 2n_f P^{qg} \\ \frac{1}{2n_f} P^{qg} & P^{gg} \end{pmatrix} (z, \alpha_s) \\ &\otimes \begin{pmatrix} D_S^h \\ D_g^h \end{pmatrix} (z, Q^2), \end{aligned} \quad (6)$$

while for the nonsinglet combination of FFs, the DGLAP equation can be written as

$$\frac{\partial}{\partial \ln Q^2} D_{NS}^h(z, Q^2) = P^+(z, \alpha_s) \otimes D_{NS}^h(z, Q^2), \quad (7)$$

where P^{ji} and P^+ are the time-like splitting functions which have a perturbative expansion in terms of the strong coupling constant α_s ,

$$P^{ji,+}(z, \alpha_s) = \sum_{l=0} a_s^{l+1} P^{ji,+ (l)}(z), \quad (8)$$

where $i, j = g, q$ and $a_s \equiv \alpha_s/(4\pi)$. The time-like splitting functions have been calculated up to $\mathcal{O}(a_s^3)$ in the $\overline{\text{MS}}$ scheme and can be found in Refs. [40–42].

The calculation of FFs in our analysis is defined in the zero-mass variable-flavor-number scheme (ZM-VFNS) where all active flavors are treated as massless quarks. Nevertheless, a dependence on the heavy-quark masses enters through the fact that the FFs for heavy-quark contributions exhibit a threshold: at scales below the heavy-quark mass the scale evolution is stopped and the FFs are kept constant. We use $m_c = 1.51$ GeV and $m_b = 4.92$ GeV for the charm and bottom thresholds, respectively. We choose $\alpha_s(M_Z) = 0.118$ as a reference value which is close to the world-average of the Particle Data Group [32].

III. METHODOLOGY AND INPUT PARAMETERIZATION

In this section we present the methodology applied in the SHKS22 analysis, namely the neural network (NN) technique, and describe the basic assumption for the input FFs parameterization. A neural network can be viewed as a complicated prescription to parametrize a function. The architecture of the network, i.e. in particular the number of layers and nodes and the way

how nodes are connected, determines the complexity of this parametrization. The typical number of parameters needed to fix a NN is around 100, or more. This is much larger than the number of parameters used in conventional approaches, where simple functional forms for FFs requires to specify in the order of 15 to 30 parameters. Therefore, NNs are expected to be much more flexible and the bias due to the choice of a specific functional form is greatly reduced. For more detailed information about the neural network approach we refer to Refs. [1, 31].

The $\Xi^- + \bar{\Xi}^+$ fragmentation functions for a parton flavor or flavor combination i in terms of a neural network is defined at the initial scale $Q_0 = 5$ GeV by

$$z D_i^{\Xi^- + \bar{\Xi}^+}(z, Q_0) = (N_i(z, \theta) - N_i(1, \theta))^2, \quad (9)$$

where $N_i(z, \theta)$ is a one-layered feed-forward neural network, and θ denotes the parameter set. The neural network architecture is $[I, N, O]$ where I is the number of input nodes, N denotes the number of intermediate nodes and O is the number of output nodes. We choose a neural network with a single input node describing the scaling variable z , a sigmoid activation function for 20 intermediate nodes and a linear activation function for 3, 5 or 6 output nodes corresponding to the flavor combinations in three different FF sets, I, II or III, respectively, which we will introduce in the following.

SIA experimental measurements are available only for the production of the sum of Ξ^- and its antiparticle $\bar{\Xi}^+$. The fragmentation structure functions in Eq. (2) do not distinguish between quark and antiquark FFs, i.e. we can only determine the combinations $D_{q^+}^h = D_q^h + D_{\bar{q}}^h$ with $h = \Xi^- + \bar{\Xi}^+$. The singlet and non-singlet combinations and the gluon FF enter with different coefficients in the SIA cross section and a separation of these three components can be expected provided data for the z and Q dependence are precise enough.

Our baseline FF parametrization, set I, is chosen assuming the following flavor combinations:

$$z D_{d^+ + s^+}^{\Xi^- + \bar{\Xi}^+}, \quad z D_{u^+ + c^+ + b^+}^{\Xi^- + \bar{\Xi}^+}, \quad z D_g^{\Xi^- + \bar{\Xi}^+}. \quad (10)$$

Since the favored quark flavors in the hadron state Ξ^- are (dss) and the value of the corresponding electroweak charges \hat{e}_q for d and s quarks are the same, we adopt the specific combination $d^+ + s^+$, as was done also in Ref. [43]. In addition we assume complete symmetry between the disfavored quarks u^+ , c^+ and b^+ . Therefore, in total we choose 3 independent flavor combinations corresponding to the neural network architecture $[1, 20, 3]$.

The FFs for up- and down-type quarks can be separated because they contribute with different charge factors to the cross section. A separation of the heavy-quark components will be possible if charm- or bottom-tagged data become available. At present, there are no heavy-flavor tagged data and it is unlikely that the precision is high enough to be useful for a further separation of flavors, beyond our ansatz described above. Nevertheless, as a test of our approach, we will also study two extended

sets, namely set II, assuming the following combinations of FFs:

$$zD_{d^++s^+}^{\Xi^-\Xi^+}, zD_{u^++\Xi^+}^{\Xi^-\Xi^+}, zD_{c^++\Xi^+}^{\Xi^-\Xi^+}, zD_{b^++\Xi^+}^{\Xi^-\Xi^+}, zD_g^{\Xi^-\Xi^+}, \quad (11)$$

where, in addition to the light quarks and the gluon, we assume separate parametrizations for the heavy quarks c^+ and b^+ , and set III where all flavors are described by different FFs:

$$zD_{d^+}^{\Xi^-/\Xi^+}, zD_{u^+}^{\Xi^-/\Xi^+}, zD_{s^+}^{\Xi^-/\Xi^+}, zD_{c^+}^{\Xi^-/\Xi^+}, zD_{b^+}^{\Xi^-/\Xi^+}, zD_g^{\Xi^-/\Xi^+} \quad (12)$$

Thus, for set II (III) we increase the number of independent distribution functions to 5 (6) and the NN architecture is $[1, 20, 5]$ ($[1, 20, 6]$). We study sets II and III in order to investigate how well FFs are restricted by data and which uncertainty could be generated by choosing a specific, possibly too general, parametrization. One can find similar approaches in the previous literature.

The number of parameters needed to specify the chosen NN architectures are 103, 145 and 166 for sets I, II and III, respectively. Due to the redundancy of these parameters inherent to the NN architecture by construction, the number of independent parameters is, however, much smaller and usually difficult to determine. Therefore we will not quote χ^2 values per degree of freedom, but rather follow the general convention and show χ^2 normalized to the number of data points when we compare the fit quality in the following.

IV. MONTE CARLO PROCEDURE AND DETERMINATION OF THE OPTIMAL FIT

There are mainly two methods used in the literature to obtain a reliable determination of the uncertainties of FFs. One of them is the iterative Hessian approach which has been used for example in the DEHSS analysis [44, 45] and has been developed in Refs. [46, 47]. The other important one, developed in Ref. [48], is the Monte Carlo procedure used in the recent JAM [7, 49] and NNFF [31] fits. We adopt the statistical framework in our SHKS22 analysis.

The **MontBlanc** framework [1] utilizes Monte Carlo together with NNs to extract information about the FFs and their uncertainty from the experimental data. The available data are used to generate a discrete sample of FF values, and NNs are employed to interpolate between data points which is needed in order to approximate the required integrations. The first step is training of the NN and creating N_{rep} replicas of NNs corresponding to pseudo-datasets. Minimization of an appropriately chosen χ^2 allows one to choose NNs such that they reproduce a probability distribution of measured points and theoretical predictions with the same mean, variance and correlation as the experimental data. We refer the reader to

Refs. [1, 31, 49, 50] and references therein for a detailed discussion of the approach.

The Monte Carlo approach assumes that the experimental data follow a multivariate Gaussian distribution,

$$\mathcal{G}(\mathbf{x}^k) \propto \exp\left((\mathbf{x}^k - \boldsymbol{\mu})^T \cdot \mathbf{C}^{-1} (\mathbf{x}^k - \boldsymbol{\mu})\right), \quad (13)$$

where $\mathbf{x}^k = \{x_1^k, x_2^k, \dots, x_{N_{\text{dat}}}^k\}$ are so called “replicas”, i.e. pseudo-datasets for a set of N_{dat} measured data points. The vector of expectation values of this distribution is $\boldsymbol{\mu}$ which corresponds to experimental data, and \mathbf{C} is the covariance matrix of the data which contains all information on the uncertainties and correlations. The elements of the covariance matrix are defined as in Ref. [1],

$$C_{ij} = \delta_{ij} \sigma_{i,\text{unc}}^2 + \sum_{\beta} \sigma_{i,\text{corr}}^{(\beta)} \sigma_{j,\text{corr}}^{(\beta)}, \quad (14)$$

where $\sigma_{i,\text{unc}}^2$ denotes the sum of squares of all uncorrelated uncertainties, such as the statistical and systematic uncertainties for the i th data point and $\sigma_{i,\text{corr}}^{(\beta)}$ is the correlated uncertainty due to β source for the same point.

The Monte Carlo approach for the uncertainty propagation uses N_{rep} replicas of the measured data, \mathbf{x}^k , to turn the experimental uncertainty into that of the NNs that parametrize the FFs. For this purpose, the covariance matrix \mathbf{C} is decomposed to a lower triangular \mathbf{L} using Cholesky method ($\mathbf{C} = \mathbf{L} \cdot \mathbf{L}^T$). If one applies this matrix to an N_{dat} -dimensional Gaussian random vector, \mathbf{r}^k , a vector with the covariance properties of the experimental data is obtained. Accordingly the pseudo-dataset is constructed as follows (by **Ceres Solver** [51]),

$$\mathbf{x}^k = \boldsymbol{\mu} + \mathbf{L} \cdot \mathbf{r}^k \quad (15)$$

This procedure ensures that for sufficiently large N_{rep} , the set of replicas satisfies the following conditions [1],

$$\frac{1}{N_{\text{rep}}} \sum_k x_i^k \simeq \mu_i, \quad \frac{1}{N_{\text{rep}}} \sum_k x_i^k x_j^k \simeq \mu_i \mu_j + C_{ij}. \quad (16)$$

At the end of the QCD analysis, a set of N_{rep} trained NNs are gained and this allows us to estimate the functional integral by averaging over the set of replicas. Notably, estimates for expectation value, uncertainty and correlation of the distribution of an observable \mathcal{D} , e.g. a cross section, is given by [50],

$$\begin{aligned} \langle \mathcal{D}(x) \rangle &= \frac{1}{N_{\text{rep}}} \sum_{k=1}^{N_{\text{rep}}} \mathcal{D}^k(x), \\ \sigma_{\mathcal{D}} &= \sqrt{\langle \mathcal{D}^2 \rangle - \langle \mathcal{D} \rangle^2}, \\ c_{\mathcal{D}}^{ij} &= \frac{\langle \mathcal{D}_i \mathcal{D}_j \rangle - \langle \mathcal{D}_i \rangle \langle \mathcal{D}_j \rangle}{\sigma_i \sigma_j}. \end{aligned} \quad (17)$$

In the SHKS22 FFs analysis, we have chosen to include $N_{\text{rep}} = 300$, although already a smaller number of replicas, say 200, could be enough to obtain a sub 1% accuracy, see Ref. [1].

V. EXPERIMENTAL DATA

The data included in our analysis is obtained from SIA measurements of the sum of cross sections for Ξ^- and $\bar{\Xi}^+$ production. We make use of all available experimental data reported by the ALEPH [9], DELPHI [10] and OPAL [11] Collaborations at CERN, the MARKII Collaboration [12] at SLAC, and the TASSO Collaboration [13, 14] at DESY. The datasets are summarized in Table I. All the data are for inclusive untagged cross-section measurements. The ALEPH, DELPHI and OPAL data are presented as multiplicities $1/\sigma_{tot}d\sigma/dx_p$ normalized to the total cross-section at the center-of-mass energy of $\sqrt{s} = M_Z$. Here, $x_p = 2|\mathbf{P}_h|/\sqrt{s}$ is the scaled hadron three-momentum. Alternatively, one can also use $z = 2E_h/\sqrt{s}$, i.e. the energy of the hadron h scaled to the beam energy $\sqrt{s}/2$. The relation between these two scaling variables is given by

$$z = x_p \sqrt{1 + \frac{4}{x_p^2} \frac{m_h^2}{s}} = 2\sqrt{\frac{m_h^2 + |\mathbf{P}_h|^2}{s}}. \quad (18)$$

The data from the MARKII and TASSO Collaborations are given in different formats. While the TASSO-34.8 data are differential cross-sections $d\sigma/dp_h$ measured at the center-of-mass energy $\sqrt{s} = 34.8$ GeV, the observables for the MARKII and TASSO-34 data are rescaled cross sections and reported for $(s/\beta)d\sigma/dz$ at the center-of-mass energies $\sqrt{s} = 29$ GeV and $\sqrt{s} = 34$ GeV, respectively. The parameter $\beta = |\mathbf{P}_h|/E_h$ is the velocity of the final state hadron h .

We select data for which a description in the framework of perturbative QCD can be expected to work well and exclude the range of very small values of z . Higher-order corrections are known to contain potentially large logarithms proportional to $\ln z$ and $\ln(1-z)$. Since the available data are limited to the range $z < 0.5$ we do not have to consider a cut for the large z region. However, we have to carefully choose a lower kinematical cut for z . In order to do so, we study the sensitivity of χ^2/N_{dat} to the variations of z_{min} at NLO accuracy. We scan z_{min} over the region $0.02 \leq z \leq 0.1$. The summary of our selection of z_{min} is presented in Table II. The first and second columns of this table show our choice of z and the remaining number of data points, respectively. The total number of data without imposing the cut is 36 points and all of these data points are used in the analysis with $z_{\text{min}} = 0.02$ cut. In the third column, we report χ^2/N_{dat} determined from the analyses with different numbers of data and minimum z cuts.

In Fig. 1, the dependence of χ^2/N_{dat} on the minimum cut value of z is presented. One can conclude from this figure that the optimal χ^2/N_{dat} value at NLO is obtained by a fit to data with $z_{\text{min}} = 0.1$. We find that there is no further improvement on χ^2/N_{dat} by increasing the number of data points and reducing z_{min} to values below 0.1. We choose the cut $z_{\text{min}} = 0.1$ for all experiments, independent of the center-of-mass energy. The number

of data points remaining after applying this cut is 27.

We note that the low- z cut, introduced to remove the region where potentially large logarithms from higher-order corrections can spoil the reliability of the theoretical predictions, allows us as well to omit corrections due to the non-zero hadron mass. Such corrections are expected to be relevant for small center-of-mass energies and in the small- z region.

VI. FF SETS AND FIT QUALITY

In this section we describe the main results of the SHKS22 analysis. We present a comparison of the $\Xi^-/\bar{\Xi}^+$ experimental data used in our analysis with the corresponding theoretical predictions calculated using our extracted SHKS22 NLO FFs and we also present a comparison of the fits at NLO and NNLO.

A detailed comparison of theoretical predictions obtained using the NLO FFs of set I with the SIA experimental data included in the fit is shown in Fig. 2. The data are shown as a function of z , limited to the range $0.1 \leq z < 0.5$ which corresponds to the cuts imposed in our selection of data to be fitted. We present both absolute values in upper panels and the ratios of theory prediction over data in lower panels. The results are shown for the ALEPH [9], DELPHI [10], OPAL [11], MARKII [12] and the TASSO Collaborations [13, 14]. Overall, one can see a very good agreement between our theory predictions and the measurements for most of the data points. We observe some deviations for the MARKII and TASSO data at $\sqrt{s} = 34$ GeV. These data points contribute substantially to χ^2 . For the case of ALEPH data, the agreement between theory predictions and data looks good; however, since the experimental errors are typically small their contribution to the total χ^2 is also large.

In Table I, introduced already above, χ^2 values per data point for each individual dataset are shown. The total χ^2 divided by the number of data points for each set is shown in the last row. All fits are acceptable. One can observe a slight increase of χ^2/N_{dat} when we go from set I to sets II and III. We have included the results for sets II and III in Fig. 2. A closer inspection of these figures shows that the differences between the three sets is mainly due to two data points, one of the ALEPH and one of the OPAL data. These points appear as outliers and their contribution to the change of χ^2 values between the three sets is particularly large.

The NLO FFs of $\Xi^- + \bar{\Xi}^+$ for set I are shown in Fig. 3 together with the corresponding uncertainty bands for the two flavor combinations $d^+ + s^+$ and $u^+ + c^+ + b^+$ and the gluon at the initial scale $Q_0 = 5$ GeV.

A comparison of the three sets of FF fits is shown in Fig. 4. Here we display the NLO results for the g , $d^+ + s^+$, and $u^+ + c^+ + b^+$ FFs at the scale $Q = M_Z$. One can see a remarkable agreement between these different sets and the differences between the central values are almost invisible in the plots. The uncertainty bands, however,

Experiment	\sqrt{s}	$N_{\text{dat}}(z > z_{\text{min}})$	χ^2/N_{dat} Set I(NLO)	χ^2/N_{dat} Set II(NLO)	χ^2/N_{dat} Set III(NLO)	χ^2/N_{dat} Set I(NNLO)
ALEPH [9]	91.2	8	1.860	2.039	2.035	1.714
DELPHI [10]	91.2	4	0.659	0.660	0.668	0.673
OPAL [11]	91.2	5	1.552	1.682	1.726	1.434
MARKII [12]	29	4	2.348	2.399	2.428	2.171
TASSO-34 [13]	34	3	1.747	1.805	1.807	1.700
TASSO-34.8 [14]	34.8	3	0.810	0.731	0.777	0.891
Total χ^2/N_{dat}		27	1.540	1.631	1.643	1.451

TABLE I: The list of input datasets for $\Xi^- + \bar{\Xi}^+$ production included in the SHKS22 analysis. For each dataset we indicate the corresponding reference and the center-of-mass energy \sqrt{s} . The number of data points N_{dat} that satisfy the kinematic cut ($z > 0.1$) is displayed in the third column. In columns 4, 5, and 6 we show the value of χ^2 per point resulting from the FF fit at NLO for set I, set II and set III, respectively. The last column shows, correspondingly, the χ^2 values for the NNLO fit. The last row contains the total values of χ^2 divided by the number of data points.

z_{min} cut	number of data points	χ^2/N_{dat}
0.02	36	4.412
0.05	34	1.967
0.075	31	2.010
0.1	27	1.540

TABLE II: The dependence on the kinematical cut, z_{min} , (first column) of the number of data points with $z > z_{\text{min}}$ analyzed in the fits (second column) and the resulting χ^2/N_{dat} in the SHKS22 fit set I at NLO.

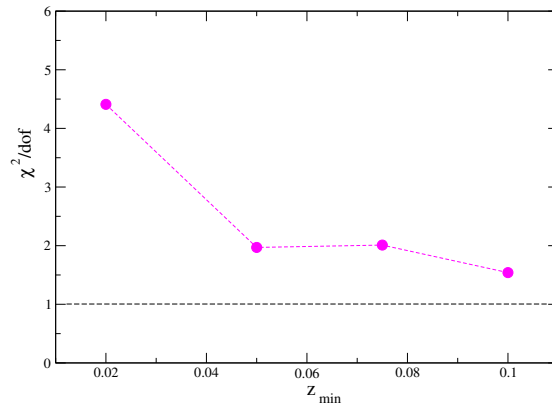


FIG. 1: Dependence of the fit quality, χ^2/N_{dat} , at NLO on the minimum cut values of z for the SIA datasets used in the SHKS22 analysis for set I.

for the $d^+ + s^+$ and $u^+ + c^+ + b^+$ combinations are wider for set I in the range of $z > 0.4$, while these FF com-

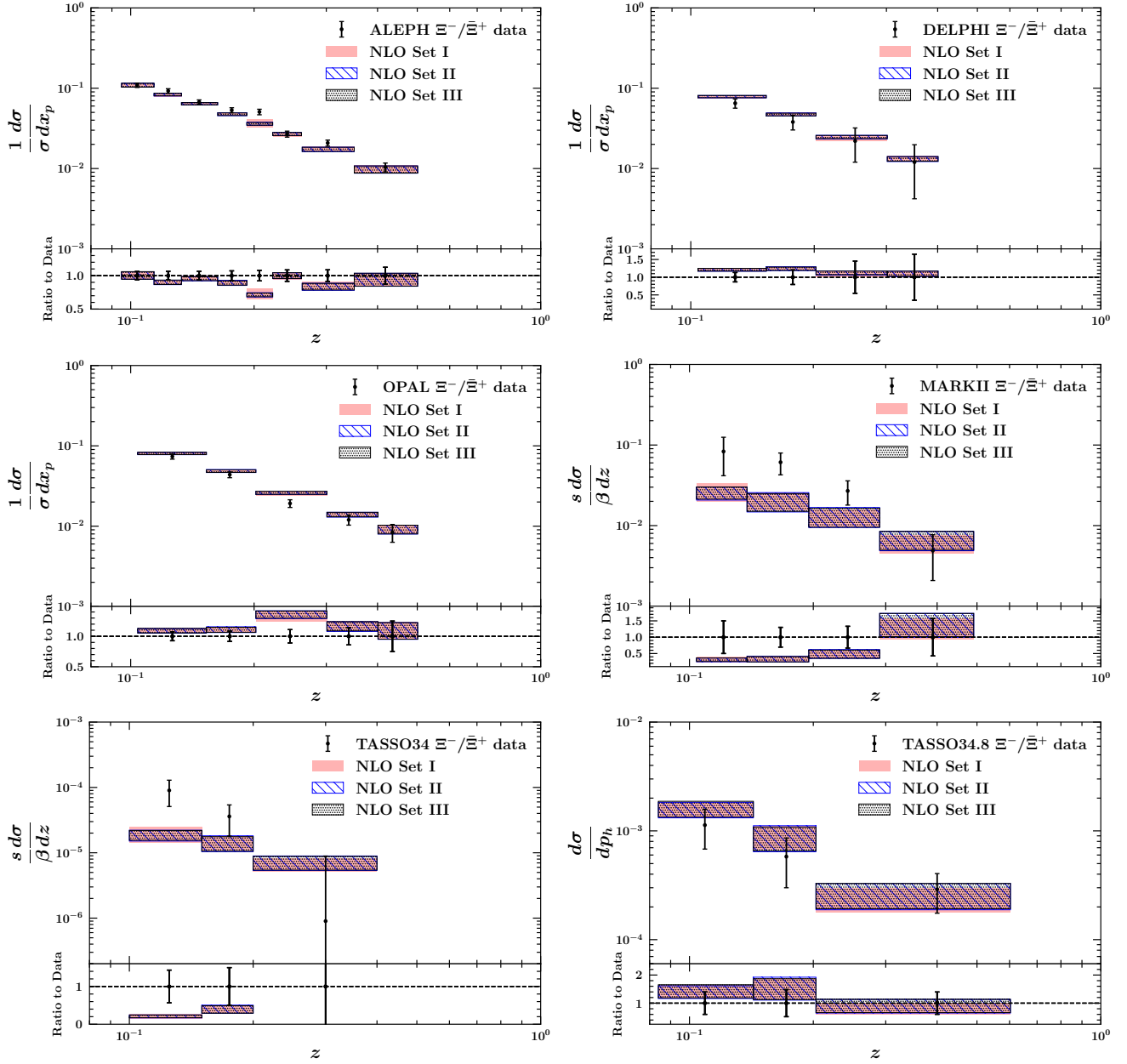


FIG. 2: NLO theory predictions and data/theory ratios for the normalized SIA cross section data. See text for details.

binations are better constrained for set I in the small z -range. In fact, the available data points cover only the range $z < 0.4$ and FF values above this range are the result of an extrapolation. We observe that the uncertainties of the gluon FF is larger than of the quark FFs for all fits. This was to be expected since the SIA data are only loosely sensitive to the gluon FF.

For sets II and III, i.e. when we allow individual flavor components of the FFs to be different, we found that the central values for the same-charge combinations, i.e. d^+ ,

s^+ and b^+ on the one hand and u^+ and c^+ on the other hand, are very similar. Therefore we do not show corresponding figures. The uncertainty bands, however, turn out to be much wider if individual components are fitted, as to be expected since the available data do not provide enough information for a separate determination of individual flavor FFs; only the corresponding sums enter the non-singlet part of the structure function F_2 in Eq. (4).

The FFs of set I contain only those flavor combinations which are needed to describe the available data, which do

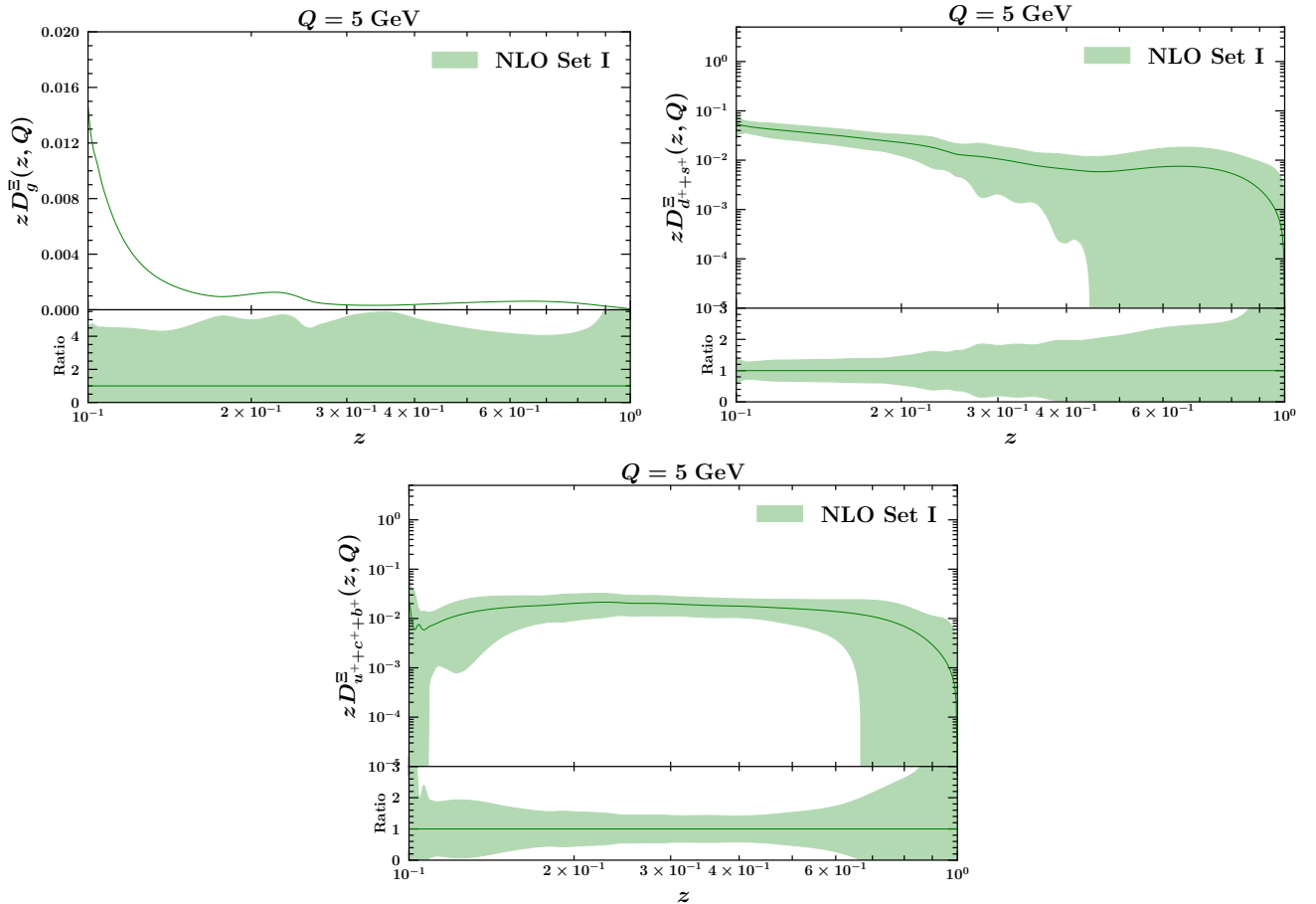


FIG. 3: The flavor combinations of set I FFs at NLO for $\Xi^- + \Xi^+$ production. Full lines describe central values, shaded areas represent corresponding uncertainty bands at the initial scale $Q_0 = 5$ GeV. The lower panels in each figure show the error bands normalized to the corresponding central values.

not distinguish light and heavy quark-initiated processes. Obviously, this is the appropriate choice to reflect the information contained in the data. Therefore we adopt set I as our baseline parametrization and present the comparison of NLO and NNLO results only for this set in the following.

A comparison of the NLO and NNLO fits for set I is shown in Fig. 5. Central values and uncertainty bands of the FFs in Fig. 5 differ only little between the NLO and NNLO calculations. The error bands overlap everywhere. Only in the large- z region, we observe some reduction of the uncertainties in the NNLO analysis. The fit quality can be judged from the χ^2 values contained in Tab. I. We observe that the NNLO fit yields improved values of χ^2/N_{dat} : 1.451 for NNLO compared with 1.540 for the NLO fit, i.e. an improvement of $\sim 10\%$. This reduction of χ^2 is shared among almost all data points except those of DELPHI and TASSO-34.8 where we observe a small increase. Overall, the inclusion of higher-order perturbative QCD corrections leads to a marginally improved set

of FFs.

VII. Ξ^-/Ξ^+ PRODUCTION AT HADRON COLLIDERS

Data for Ξ^-/Ξ^+ production at hadron colliders, $p\bar{p}$ scattering at the Tevatron and pp collisions at the LHC, are presently available only at very low values of the transverse momentum, p_T . Perturbative QCD is not expected to work reliably in this p_T range and a description in a picture assuming independent parton-to-hadron fragmentation is possibly missing dominating non-perturbative effects. In order to separate such non-perturbative effects and identify possible collective phenomena, which could become important for example in the hot quark-gluon plasma in heavy-ion collisions, it will be important to compare data with predictions in a framework using FFs obtained at high energy scales and extrapolating down into the p_T range where data al-

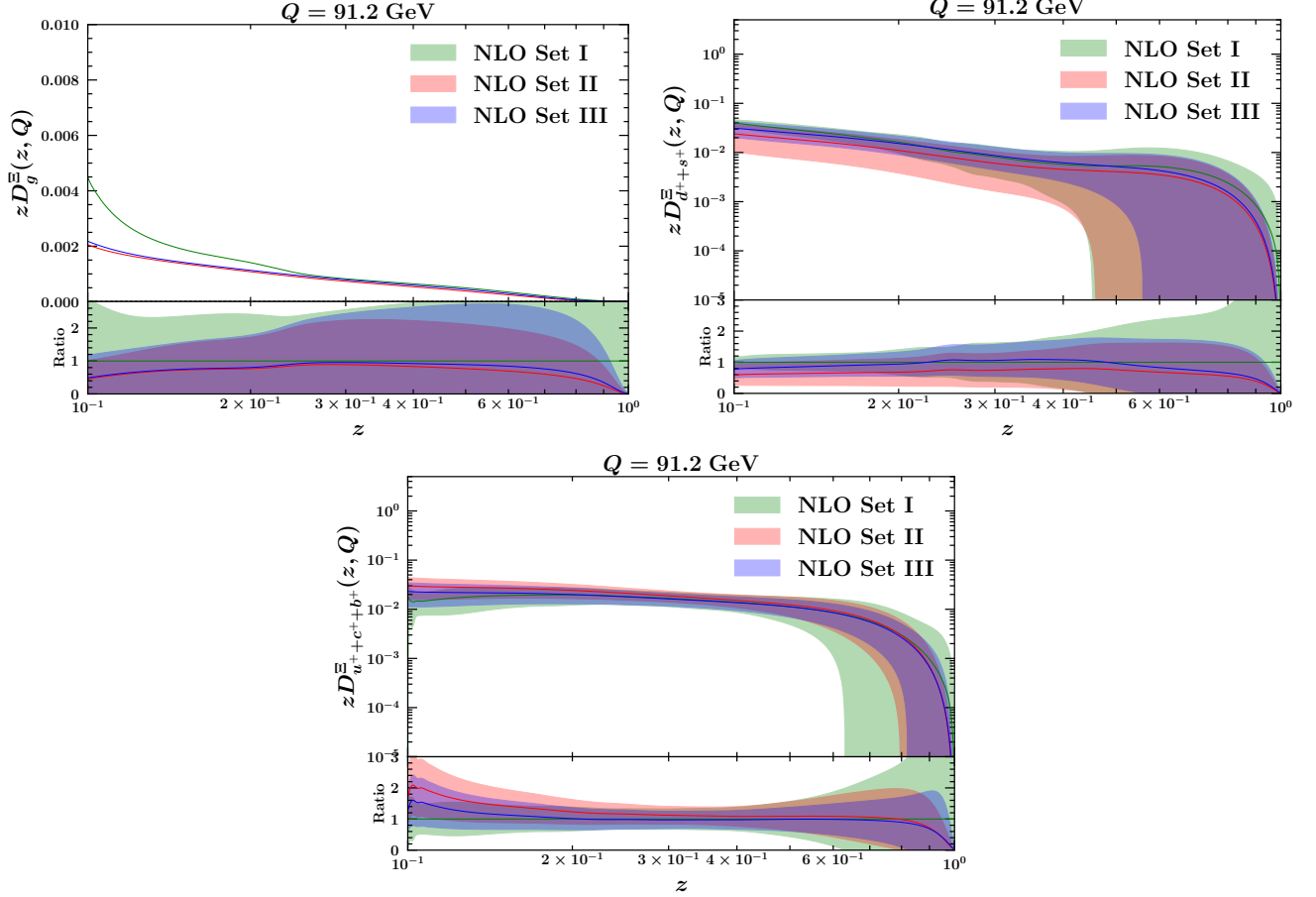


FIG. 4: Comparison of the FFs of set I, II and III at the scale $Q = M_Z = 91.2$ GeV. We display the NLO results for $\Xi^- + \bar{\Xi}^+$ FFs, $zD_i^{\Xi^- + \bar{\Xi}^+}(z)$ ($i = g, d^+ + s^+, u^+ + c^+ + b^+$).

ready exist. On the other hand, future measurements at the LHC experiments at higher p_T can eventually contribute to an improved determination of the $\Xi^- + \bar{\Xi}^+$ FFs.

Hadron production in pp and $p\bar{p}$ collisions are sensitive to relatively large z values while the available data from SIA are restricted to $z < 0.5$. To some extent, our predictions are therefore based on extrapolating the $\Xi^- + \bar{\Xi}^+$ FFs into a yet unconstrained kinematic range. We have checked, however, that the hadron collider cross sections described below do have some overlap with the SIA data: about 20 % of the pp and $p\bar{p}$ cross sections originate from the region with $z < 0.5$.

Here we show results of the calculation of cross sections for collider experiments.

The calculation is done with code that was originally developed for the production of heavy quarks (`gmvfns-3.4`, described in Ref. [52]), but adapted for massless quarks for the present purpose. It is based on the results of the calculation of Ref. [53] which includes

next-to-leading order corrections and takes into account all sub-processes with incoming and outgoing quarks and gluons. In order to connect our results with the existing data, we compare with measurements in $p\bar{p}$ collisions from CDF [18] at $\sqrt{s} = 1.96$ TeV in the rapidity range $|y| \leq 1$, as well as in pp collisions from CMS [20] at $\sqrt{s} = 5.02$ TeV, $|y| \leq 1.8$ and from ALICE [23] at $\sqrt{s} = 13$ TeV, $|y| \leq 0.5$. Results are shown in Fig. 6, compared with the existing data in the p_T range up to about 6 – 8 GeV and predictions extending up to $p_T = 20$ GeV. The default predictions, using the CT18nlo set of parton distributions from [54, 55] and the central member of the set I $\Xi^- + \bar{\Xi}^+$ FFs turn out to be considerably smaller than the data, as expected.

There are two important sources for uncertainties of the theoretical predictions: variations of the renormalization and the factorization scales, and uncertainties due to the FF parametrization. Renormalization and factorization scales have been set equal to p_T in our default predictions. The short-dashed lines in Fig. 6 show

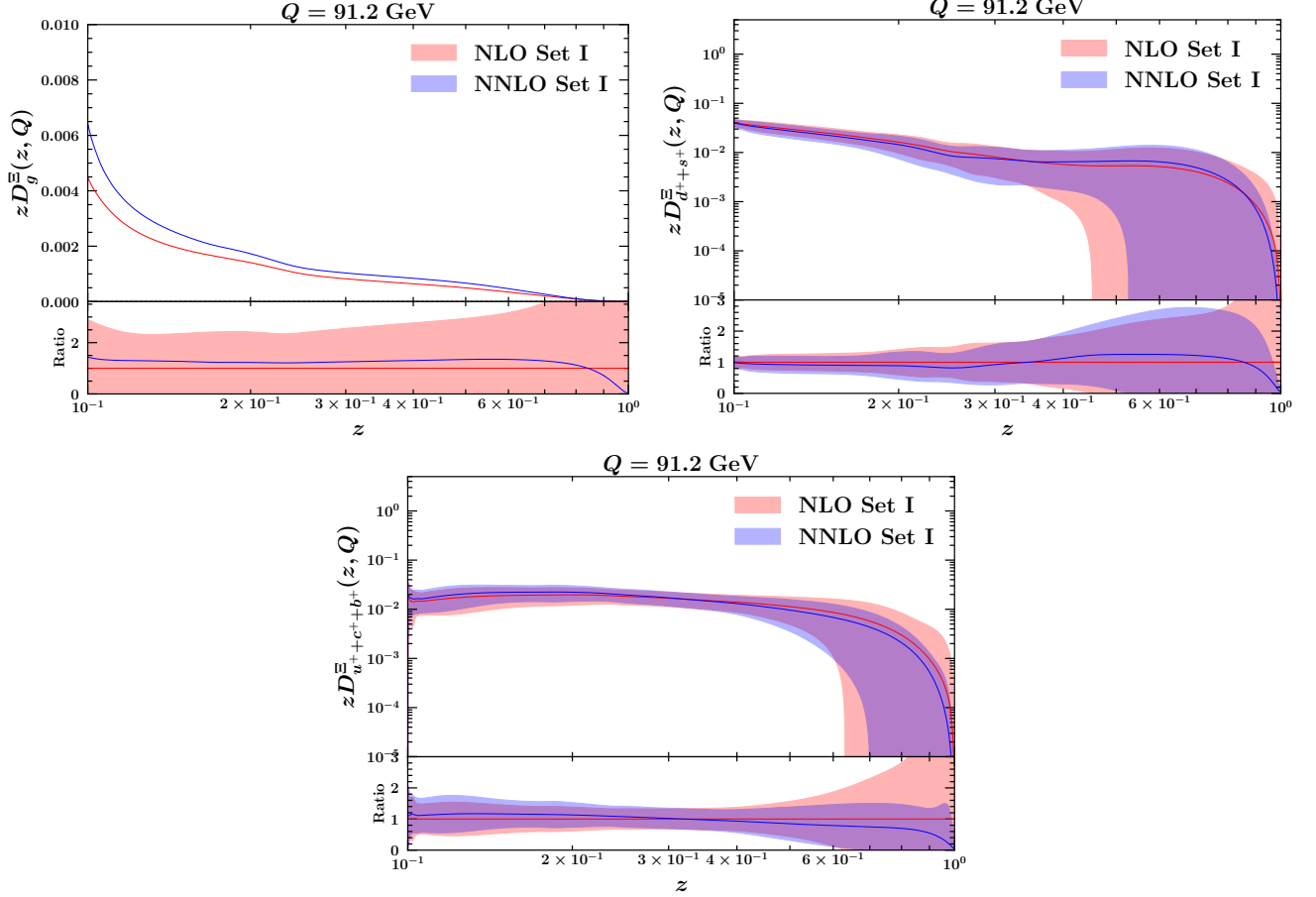


FIG. 5: Comparison of the NLO and NNLO versions of the $\Xi^- + \bar{\Xi}^+$ FFs for the flavor combinations of set I at the scale $Q = M_Z$.

the error band due to variations of the renormalization scale by factors of 2 up and down. The uncertainty from variations of the factorization scales is always smaller than that due to variations of the renormalization scale. The uncertainty from the FF parametrization is, however, dominating. This is shown by the long-dash-dotted (green) lines in Fig. 6. The corresponding error band is obtained by scanning over 300 replicas of the $\Xi^- + \bar{\Xi}^+$ FFs. The predicted cross sections follow an asymmetric distribution with a mean value much smaller than the result from the central FF. The error band shown in Fig. 6 covers the 1σ -range, obtained by excluding the lowest and highest 16% of predicted cross section values [56]. Obviously, with FFs from our present SHKS22 analysis, there are very large uncertainties. In turn, this means that future measurements at the LHC can be expected to provide valuable information to further constrain the FF parametrization for $\Xi^- + \bar{\Xi}^+$ hadron production. This will be particularly important for the gluon FF for which our fits with presently available data resulted in large un-

certainties. In contrast to SIA data, the measurements at hadron colliders are dominated by the gluon-to- Ξ FF: about 70% of the cross section is due to this FF component. Therefore one can expect considerably reduced uncertainties of the gluon FF from future LHC data.

VIII. SUMMARY AND CONCLUSIONS

In this paper we have introduced a new set of unpolarized FFs for $\Xi^-/\bar{\Xi}^+$ production, called SHKS22. This analysis presents the first precise determination of $\Xi^-/\bar{\Xi}^+$ fragmentation functions which include higher-order perturbative corrections at NNLO accuracy. The current analysis is based on a comprehensive dataset from single inclusive electron-positron annihilation experiments. We found that including data points in the region of $z \geq 0.1$ allows us to obtain stable fit results.

We have explored three different FF sets and parametrized them in terms of Neural Networks. This

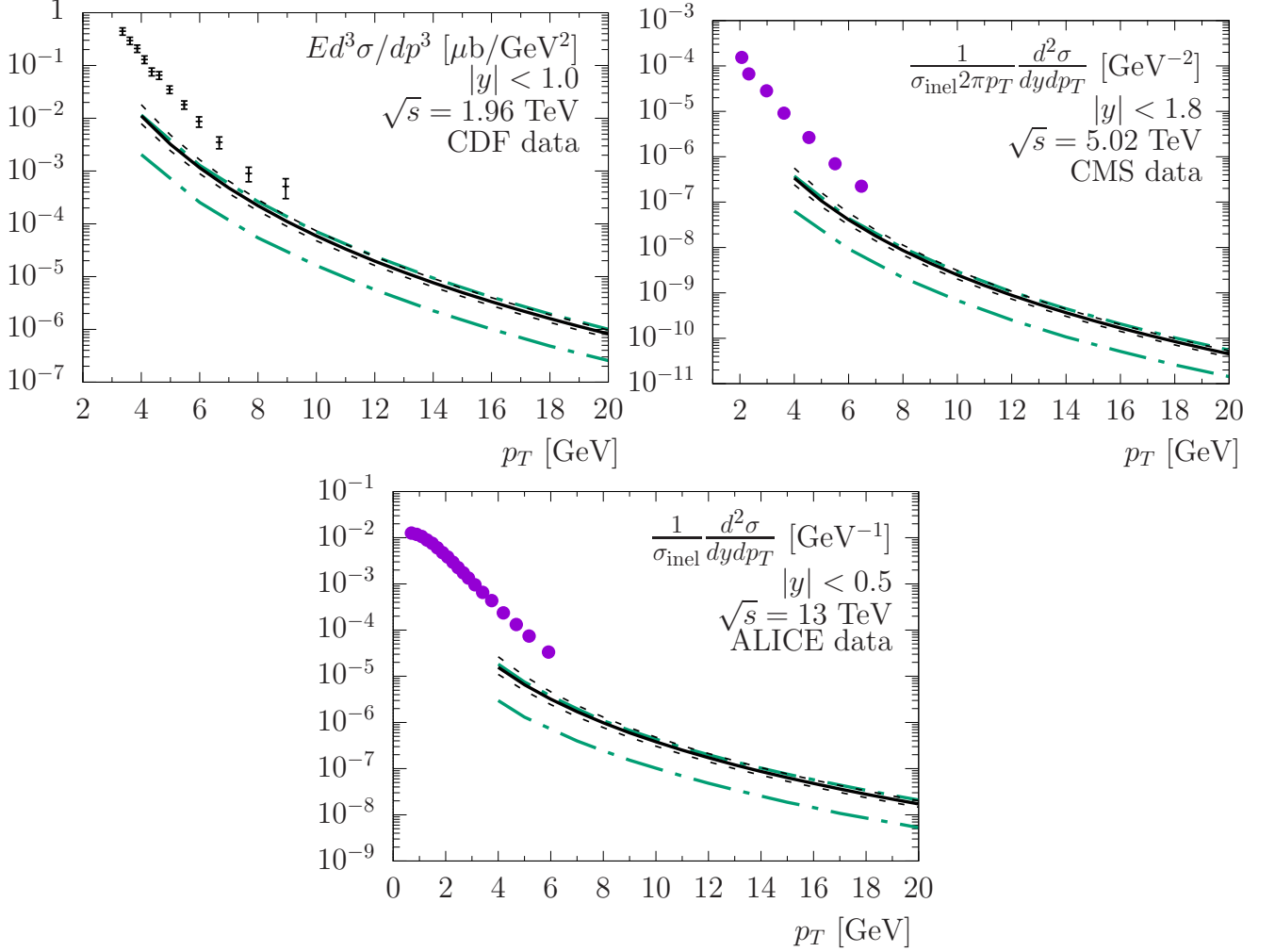


FIG. 6: Predictions for $\Xi^- + \Xi^+$ production at hadron colliders: CDF at the Tevatron [18], CMS [20] and ALICE [23] at the LHC. In the case of CMS and ALICE, data points have been read off from the corresponding published figures and error bars are not shown since they are too small to be reliably extracted from the figures. Parton distributions from [54, 55], set CT18nlo, were used and theory errors are shown as described in the text.

approach is expected to lead to a substantial reduction of theoretical bias in the choice of a parametrization. The parameters describing the Neural Networks are fitted to the SIA data. We have used the recent publicly available package **MontBlanc** to set up the parametrization of FFs, perform their evolution and calculate the SIA production cross-sections. In addition, a Monte Carlo sampling method is used to propagate the experimental uncertainties into the fitted FFs and to calculate the uncertainties for FFs and corresponding observables.

All three sets of FFs obtained in this work describe the SIA experimental data reasonably well. Our baseline set I contains a minimal choice of parameters describing the sum of favored quark flavors $d^+ + s^+$ and assumes symmetry between the disfavored quark flavors u^+ , c^+ and b^+ .

The available data do not provide enough information to obtain precise FFs for each quark flavor separately.

Our new results provide an important ingredient needed for the calculation of theoretical predictions for the hadron production in proton-proton collisions. We have used our FFs to calculate the inclusive $\Xi^- + \Xi^+$ baryon production in proton-proton collisions, extending the presently covered transverse momentum range of the CDF, CMS and ALICE measurements. Corresponding future measurements can then be used to extract $\Xi^- + \Xi^+$ FFs in combination with SIA data.

The main result of this work, i.e. the $\Xi^- + \Xi^+$ FFs, are available as grid files formatted for the LHAPDF library from the authors upon request.

ACKNOWLEDGMENTS

The authors are thankful to Valerio Bertone for many helpful discussions and comments. M.S., H.H. and H.K. thank the School of Particles and Accelerators, Institute for Research in Fundamental Sciences (IPM) for financial support provided for this research. M. S. is thankful to the Iran Science Elites Federation for the financial support. H.K. is thankful to the Department of Physics at the University of Udine and International Centre for Theoretical Physics (ICTP) for the financial support provided for this research.

-
- [1] R. A. Khalek, V. Bertone and E. R. Nocera, “Determination of unpolarized pion fragmentation functions using semi-inclusive deep-inelastic-scattering data,” *Phys. Rev. D* **104**, no.3, 034007 (2021).
- [2] H. Abdolmaleki *et al.* [xFitter Developers’ Team], “QCD analysis of pion fragmentation functions in the xFitter framework,” *Phys. Rev. D* **104**, no.5, 056019 (2021).
- [3] Z. B. Kang, A. Prokudin, P. Sun and F. Yuan, “Extraction of Quark Transversity Distribution and Collins Fragmentation Functions with QCD Evolution,” *Phys. Rev. D* **93**, no.1, 014009 (2016).
- [4] M. Soleymaninia and H. Khanpour, “Transverse momentum dependent of charged pion, kaon, and proton/antiproton fragmentation functions from e^+e^- annihilation process,” *Phys. Rev. D* **100**, no.9, 094033 (2019).
- [5] B. A. Kniehl, G. Kramer, I. Schienbein and H. Spiesberger, “ Λ_c^\pm production in pp collisions with a new fragmentation function,” *Phys. Rev. D* **101**, no.11, 114021 (2020).
- [6] P. Zurita, “Medium modified Fragmentation Functions with open source xFitter,” [arXiv:2101.01088 \[hep-ph\]](https://arxiv.org/abs/2101.01088).
- [7] E. Moffat *et al.* [Jefferson Lab Angular Momentum (JAM)], “Simultaneous Monte Carlo analysis of parton densities and fragmentation functions,” *Phys. Rev. D* **104**, no.1, 016015 (2021).
- [8] E. C. Aschenauer, I. Borsa, R. Sassot and C. Van Hulse, “Semi-inclusive Deep-Inelastic Scattering, Parton Distributions and Fragmentation Functions at a Future Electron-Ion Collider,” *Phys. Rev. D* **99**, no.9, 094004 (2019).
- [9] R. Barate *et al.* [ALEPH], “Studies of quantum chromodynamics with the ALEPH detector,” *Phys. Rept.* **294**, 1-165 (1998).
- [10] P. Abreu *et al.* [DELPHI], “Strange baryon production in Z hadronic decays,” *Z. Phys. C* **67**, 543-554 (1995).
- [11] G. Alexander *et al.* [OPAL], “Strange baryon production in hadronic Z0 decays,” *Z. Phys. C* **73**, 569-586 (1997).
- [12] S. Klein, T. Himel, G. S. Abrams, D. Amidei, A. R. Baden, T. Barklow, A. Boyarski, J. Boyer, P. Burchat and D. L. Burke, *et al.* “Observation of Ξ^- Production in e^+e^- Annihilation at 29-GeV,” *Phys. Rev. Lett.* **58**, 644 (1987).
- [13] M. Althoff *et al.* [TASSO], “Observation of Xi-, Anti-xi- Production in e^+e^- Annihilation,” *Phys. Lett. B* **130**, 340-344 (1983).
- [14] W. Braunschweig *et al.* [TASSO], “Strange Baryon Production in e^+e^- Annihilation,” *Z. Phys. C* **45**, 209 (1989).
- [15] A. Aduszkiewicz *et al.* [NA61/SHINE], “Measurements of Ξ^- and Ξ^+ production in proton-proton interactions at $\sqrt{s_{NN}} = 17.3$ GeV in the NA61/SHINE experiment,” *Eur. Phys. J. C* **80**, no.9, 833 (2020).
- [16] B. I. Abelev *et al.* [STAR], “Strange particle production in p+p collisions at $s^{*}(1/2) = 200$ -GeV,” *Phys. Rev. C* **75**, 064901 (2007).
- [17] M. Heinz [STAR], “How important are next-to-leading order models in predicting strange particle spectra in p + p collisions at STAR?,” *Eur. Phys. J. C* **49**, 129-133 (2007).
- [18] T. Aaltonen *et al.* [CDF], “Production of Λ , $\bar{\Lambda}^0$, Ξ^\pm and Ω^\pm Hyperons in $p\bar{p}$ Collisions at $\sqrt{s} = 1.96$ TeV,” *Phys. Rev. D* **86**, 012002 (2012).
- [19] V. Khachatryan *et al.* [CMS], “Strange Particle Production in pp Collisions at $\sqrt{s} = 0.9$ and 7 TeV,” *JHEP* **05**, 064 (2011).
- [20] A. M. Sirunyan *et al.* [CMS], “Strange hadron production in pp and pPb collisions at $\sqrt{s_{NN}} = 5.02$ TeV,” *Phys. Rev. C* **101**, no.6, 064906 (2020).
- [21] B. Abelev *et al.* [ALICE], “Multi-strange baryon production in pp collisions at $\sqrt{s} = 7$ TeV with ALICE,” *Phys. Lett. B* **712**, 309-318 (2012).
- [22] S. Acharya *et al.* [ALICE], “Multiplicity dependence of (multi-)strange hadron production in proton-proton collisions at $\sqrt{s} = 13$ TeV,” *Eur. Phys. J. C* **80**, no.2, 167 (2020).
- [23] S. Acharya *et al.* [ALICE], “Production of light-flavor hadrons in pp collisions at $\sqrt{s} = 7$ and $\sqrt{s} = 13$ TeV,” *Eur. Phys. J. C* **81**, no.3, 256 (2021).
- [24] C. Bourrely and J. Soffer, “Statistical approach for unpolarized fragmentation functions for the octet baryons,” *Phys. Rev. D* **68**, 014003 (2003).
- [25] J. Rafelski and B. Muller, “Strangeness Production in the Quark-Gluon Plasma,” *Phys. Rev. Lett.* **48**, 1066 (1982) [erratum: *Phys. Rev. Lett.* **56**, 2334 (1986)].
- [26] P. Koch, B. Müller and J. Rafelski, “From Strangeness Enhancement to Quark-Gluon Plasma Discovery,” *Int. J. Mod. Phys. A* **32**, no.31, 1730024 (2017) [arXiv:1708.08115 [nucl-th]].
- [27] B. Abelev *et al.* [ALICE], “Centrality dependence of π , K, p production in Pb-Pb collisions at $\sqrt{s_{NN}} = 2.76$ TeV,” *Phys. Rev. C* **88**, 044910 (2013) [arXiv:1303.0737 [hep-ex]].
- [28] I. G. Bearden *et al.* [NA44], “Collective expansion in high-energy heavy ion collisions,” *Phys. Rev. Lett.* **78**, 2080-2083 (1997).
- [29] <https://github.com/MapCollaboration/MontBlanc>.
- [30] R. D. Ball *et al.* [NNPDF], “Parton distributions from high-precision collider data,” *Eur. Phys. J. C* **77**, no.10, 663 (2017).
- [31] V. Bertone *et al.* [NNPDF], “A determination of the fragmentation functions of pions, kaons, and protons with faithful uncertainties,” *Eur. Phys. J. C* **77**, no.8, 516 (2017).
- [32] M. Tanabashi *et al.* [Particle Data Group], “Review of Particle Physics,” *Phys. Rev. D* **98**, no.3, 030001 (2018).
- [33] R. K. Ellis, W. J. Stirling, and B. R. Webber, *QCD and Collider Physics*, Cambridge University Press (1996).
- [34] P. J. Rijken and W. L. van Neerven, “Higher order QCD corrections to the transverse and longitudinal fragmentation functions in electron - positron annihilation,” *Nucl. Phys. B* **487**, 233-282 (1997) doi:10.1016/S0550-3213(96)00669-4 [arXiv:hep-ph/9609377 [hep-ph]].
- [35] P. J. Rijken and W. L. van Neerven, “O (α_s^{*2}) contributions to the asymmetric fragmentation function in e^+e^- annihilation,” *Phys. Lett. B* **392**, 207-215 (1997).
- [36] J. Blumlein and V. Ravindran, “O ($\alpha_s^{*2}(s)$) Timelike Wilson Coefficients for Parton-Fragmentation Functions in Mellin Space,” *Nucl. Phys. B* **749**, 1-24 (2006).
- [37] V. N. Gribov and L. N. Lipatov, “Deep inelastic e p scattering in perturbation theory,” *Sov. J. Nucl. Phys.* **15**, 438-450 (1972).
- [38] G. Altarelli and G. Parisi, “Asymptotic Freedom in Parton Language,” *Nucl. Phys. B* **126**, 298-318 (1977).

- [39] Y. L. Dokshitzer, “Calculation of the Structure Functions for Deep Inelastic Scattering and e^+e^- Annihilation by Perturbation Theory in Quantum Chromodynamics,” *Sov. Phys. JETP* **46**, 641-653 (1977).
- [40] A. Mitov, S. Moch and A. Vogt, “Next-to-Next-to-Leading Order Evolution of Non-Singlet Fragmentation Functions,” *Phys. Lett. B* **638**, 61-67 (2006).
- [41] S. Moch and A. Vogt, “On third-order timelike splitting functions and top-mediated Higgs decay into hadrons,” *Phys. Lett. B* **659**, 290-296 (2008).
- [42] A. A. Almasy, S. Moch and A. Vogt, “On the Next-to-Next-to-Leading Order Evolution of Flavour-Singlet Fragmentation Functions,” *Nucl. Phys. B* **854**, 133-152 (2012).
- [43] J. Binnewies, B. A. Kniehl and G. Kramer, “Next-to-leading order fragmentation functions for pions and kaons,” *Z. Phys. C* **65**, 471-480 (1995).
- [44] D. de Florian, R. Sassot, M. Epele, R. J. Hernández-Pinto and M. Stratmann, “Parton-to-Pion Fragmentation Reloaded,” *Phys. Rev. D* **91**, no.1, 014035 (2015).
- [45] D. de Florian, M. Epele, R. J. Hernandez-Pinto, R. Sassot and M. Stratmann, “Parton-to-Kaon Fragmentation Revisited,” *Phys. Rev. D* **95**, no.9, 094019 (2017).
- [46] J. Pumplin, D. R. Stump and W. K. Tung, “Multivariate fitting and the error matrix in global analysis of data,” *Phys. Rev. D* **65**, 014011 (2001).
- [47] J. Pumplin, D. Stump, R. Brock, D. Casey, J. Huston, J. Kalk, H. L. Lai and W. K. Tung, “Uncertainties of predictions from parton distribution functions. 2. The Hessian method,” *Phys. Rev. D* **65**, 014013 (2001).
- [48] N. Sato *et al.* [Jefferson Lab Angular Momentum], “Iterative Monte Carlo analysis of spin-dependent parton distributions,” *Phys. Rev. D* **93**, no.7, 074005 (2016).
- [49] N. Sato, J. J. Ethier, W. Melnitchouk, M. Hirai, S. Kumano and A. Accardi, “First Monte Carlo analysis of fragmentation functions from single-inclusive e^+e^- annihilation,” *Phys. Rev. D* **94**, no.11, 114004 (2016).
- [50] S. Forte, L. Garrido, J. I. Latorre and A. Piccione, “Neural network parametrization of deep inelastic structure functions,” *JHEP* **05**, 062 (2002).
- [51] S. Agarwal, K. Mierle, and Others, “Ceres solver.” <http://ceres-solver.org>.
- [52] B. A. Kniehl, G. Kramer, I. Schienbein and H. Spiesberger, “Collinear subtractions in hadroproduction of heavy quarks,” *Eur. Phys. J. C* **41**, 199-212 (2005).
- [53] F. Aversa, P. Chiappetta, M. Greco and J. P. Guillet, “QCD Corrections to Parton-Parton Scattering Processes,” *Nucl. Phys. B* **327**, 105 (1989).
- [54] T. J. Hou, K. Xie, J. Gao, S. Dulat, M. Guzzi, T. J. Hobbs, J. Huston, P. Nadolsky, J. Pumplin and C. Schmidt, *et al.* “Progress in the CTEQ-TEA NNLO global QCD analysis,” [arXiv:1908.11394 \[hep-ph\]](https://arxiv.org/abs/1908.11394).
- [55] T. J. Hou, J. Gao, T. J. Hobbs, K. Xie, S. Dulat, M. Guzzi, J. Huston, P. Nadolsky, J. Pumplin and C. Schmidt, *et al.* “New CTEQ global analysis of quantum chromodynamics with high-precision data from the LHC,” *Phys. Rev. D* **103**, no.1, 014013 (2021).
- [56] J. Butterworth, S. Carrazza, A. Cooper-Sarkar, A. De Roeck, J. Feltesse, S. Forte, J. Gao, S. Glazov, J. Huston and Z. Kassabov, *et al.* “PDF4LHC recommendations for LHC Run II,” *J. Phys. G* **43**, 023001 (2016).